Mast cell chymase has a negative impact on human osteoblasts

Thomas Lind [a], **Fabio Rabelo Melo** [b], **Ann-Marie Gustafson** [a,b], **Anders Sundqvist** [c], **Xinran O Zhao** [b], **Aristidis Moustakas** [b], **Håkan Melhus** [a] and **Gunnar Pejler** [b]

***a* - Uppsala University Hospital,** *Department of Medical Sciences, Section of Clinical Pharmacology, Uppsala, Sweden*
***b* - Uppsala University,** *Department of Medical Biochemistry and Microbiology, Uppsala, Sweden*
***c* - Uppsala University,** *Department of Medical Biochemistry and Microbiology, Science for Life Laboratory, Uppsala, Sweden*

Corresponding to Thomas Lind: *Uppsala University Hospital, Department of Medical Sciences, Section of Clinical Pharmacology, Uppsala, Sweden. thomas.lind@medsci.uu.se.*
https://doi.org/10.1016/j.matbio.2022.07.005

Abstract

Mast cells have been linked to osteoporosis and bone fractures, and in a previous study we found that mice lacking a major mast cell protease, chymase, develop increased diaphyseal bone mass. These findings introduce the possibility that mast cell chymase can regulate bone formation, but the underlying mechanism(s) has not previously been investigated. Here we hypothesized that chymase might exert such effects through a direct negative impact on osteoblasts, i.e., the main bone-building cells. Indeed, we show that chymase has a distinct impact on human primary osteoblasts. Firstly, chymase was shown to have pronounced effects on the morphological features of osteoblasts, including extensive cell contraction and actin reorganization. Chymase also caused a profound reduction in the output of collagen from the osteoblasts, and was shown to degrade osteoblast-secreted fibronectin and to activate pro-matrix metallopeptidase-2 released by the osteoblasts. Further, chymase was shown to have a preferential impact on the gene expression, protein output and phosphorylation status of TGFβ-associated signaling molecules. A transcriptomic analysis was conducted and revealed a significant effect of chymase on several genes of importance for bone metabolism, including a reduction in the expression of osteoprotegerin, which was confirmed at the protein level. Finally, we show that chymase interacts with human osteoblasts and is taken up by the cells. Altogether, the present findings provide a functional link between mast cell chymase and osteoblast function, and can form the basis for a further evaluation of chymase as a potential target for intervention in metabolic bone diseases.
© 2022 The Author(s). Published by Elsevier B.V. This is an open access article under the CC BY license (http://creativecommons.org/licenses/by/4.0/)

Introduction

Fractures of the skeleton, especially at the hip, represent devastating injuries, resulting in disability, increased mortality and high treatment costs. The risk of hip fractures increases with age and, as a consequence of the aging human population, the incidence of fractures is expected to increase within the society [1]. To improve the effectiveness of treatments to prevent fractures, there is a large need for identifying novel mechanisms operative in bone homeostasis (especially those promoting bone growth), thereby forming the basis for developing better ways to improve bone strength [2, 3].

Mast cells are well known for their detrimental impact in allergic disorders, but there is a rising awareness of a role for mast cells in various additional pathologies, including, e.g., fibrosis, atherosclerosis, cancer, obesity and diseases of the skeletal system [4–7]. As an example of the latter, bone marrow mast cells are increased in osteoporosis and in hyperparathyroidism [8, 9]. Further, reduced bone quality, with or without fragility fractures, is a common feature of mastocytosis, particularly in men [10–14]. It has been demonstrated that bone biopsies from such patients show increased mast cell numbers, correlating with reduced bone volume [11]. Further, mast cells are more often found close to osteoblasts than osteoclasts

0945-053X/© 2022 The Author(s). Published by Elsevier B.V. This is an open access article under the CC BY license (http://creativecommons.org/licenses/by/4.0/)

in such settings, which is contrary to what is observed in multiple myeloma or metastatic foci, where cancer cells are found close to osteoclasts [9, 15].

In line with an impact of mast cells on bone remodeling, studies in animal models of osteoporosis, hyperparathyroidism, fracture healing and heterotopic ossification have revealed a close association between bone homeostasis and mast cell numbers [16–19]. Further, teriparatide (recombinant parathyroid hormone (PTH)), a bone-anabolic drug given intermittently to patients with severe osteoporosis, was shown to reduce mast cell numbers in mice [19].

Among the various preformed compounds stored in the mast cell secretory granules [20–22], chymases are particularly abundant, accounting for up to 25% of the total cellular protein [23, 24]. Chymases are mast cell-restricted serine proteases that can cleave a large number of proteins/peptides [25]. In humans, only one chymase gene is expressed (CMA1), and mice lacking the functional homologue to CMA1 (Mcpt4$^{-/-}$) are known to develop less severe disease in various animal models (reviewed in [25]). In addition, we have shown that ablation of chymase (Mcpt4) in mice induced a persistent expansion of diaphyseal bone in comparison with wild type controls [26]. Importantly, these effects were observed under baseline conditions, suggesting that chymase can have an effect on normal bone homeostasis. Moreover, this effect was only seen in female mice [26] and, in line with an impact of chymase on bone mass in females, mast cells derived from female mice express higher chymase levels than cells from males [27]. Based on these findings, chymase can thereby be considered as a potential drug target in strategies to increase bone mass, with possible applications for treatment of osteoporosis and other diseases characterized by bone degeneration.

Although previous findings have implicated mast cell chymase in the regulation of bone generation, the underlying mechanism is unknown. Here we addressed this issue by exploring the possibility that mast cell chymase might regulate the functionality of human osteoblasts. Indeed, our findings revealed that chymase had dramatic effects on multiple features of primary human osteoblasts, thereby providing novel insight into how mast cells can impact on bone remodeling.

Results

Human recombinant chymase induces contraction of primary human osteoblasts

To approach the mechanism by which chymase affects bone homeostasis [26], we reasoned that the main bone-forming cells, i.e., osteoblasts, could be affected by chymase. To address this possibility, human primary osteoblasts were recovered during knee replacement surgery, and were exposed to recombinant human chymase under serum-free conditions (serum contains protease inhibitors to which chymase is sensitive [28–30]). As seen in Fig. 1A, chymase (50 nM) caused dramatic morphological effects on the osteoblasts, as manifested by a marked contraction of the cells. This effect was seen at chymase concentrations down to 1.6 nM (Suppl. Fig. 1) and was first observed ~10 min after addition of chymase. Suppl. Video shows the kinetics and real-time assessment of how chymase affects the morphology of osteoblasts. In contrast, mast cell tryptase, i.e., another major protease stored in the mast cell secretory granules [22], had no impact on osteoblast morphology (Fig. 1A). Upon reintroduction of serum, the morphological changes were reversed and cells regained normal morphology (Fig. 1B and Suppl. Video). This indicates that the effects of chymase on osteoblasts were reversible. In agreement with the effects of chymase on the human primary osteoblasts, a mouse osteoblast cell line was also affected in a similar fashion (Fig. 1A). As shown by assessment of cell death markers (Annexin V, DRAQ7) by flow cytometry, chymase did not cause cell death of the osteoblasts (Fig. 1C). Hence, mast cell chymase had a major morphological impact on human osteoblasts, without causing any detectable effects on cellular viability.

The effects of chymase on osteoblast morphology could potentially be dependent on effects of chymase on compounds to which to which the osteoclasts adhere. To test this possibility, cell culture wells were either non-coated or coated with fibronectin or collagen, followed by treatment with chymase and subsequent seeding of the cells. As seen in Suppl. Fig. 2, pre-treatment of the wells with chymase did not affect the ability of the osteoblasts to adhere or spread. Hence, these findings indicate that the effects of chymase on osteoblast morphology are most likely due to direct effects on the cells rather than to effects on their supporting matrix.

To assess whether the effects of chymase on the osteoblasts were dependent on its catalytic activity, we performed experiments where the enzymatic activity of chymase was inhibited by chymostatin. As seen in Suppl. Fig. 3, the effects of chymase on the osteoblasts were completely abolished when chymase had been pre-treated for 15 min with chymostatin, indicating that the ability of chymase to affect osteoblasts was dependent on its catalytic activity. However, this effect was ameliorated after prolonged culture, possibly reflecting that chymostatin is a reversible protease inhibitor. Chymase is highly positively charged and it is known that heparin, a highly negatively charged glycosaminoglycan, binds strongly to chymase [31]. To address whether such an interaction can influence the capacity of chymase to affect osteoblasts, we performed experiments where chymase was added to the osteoblasts either

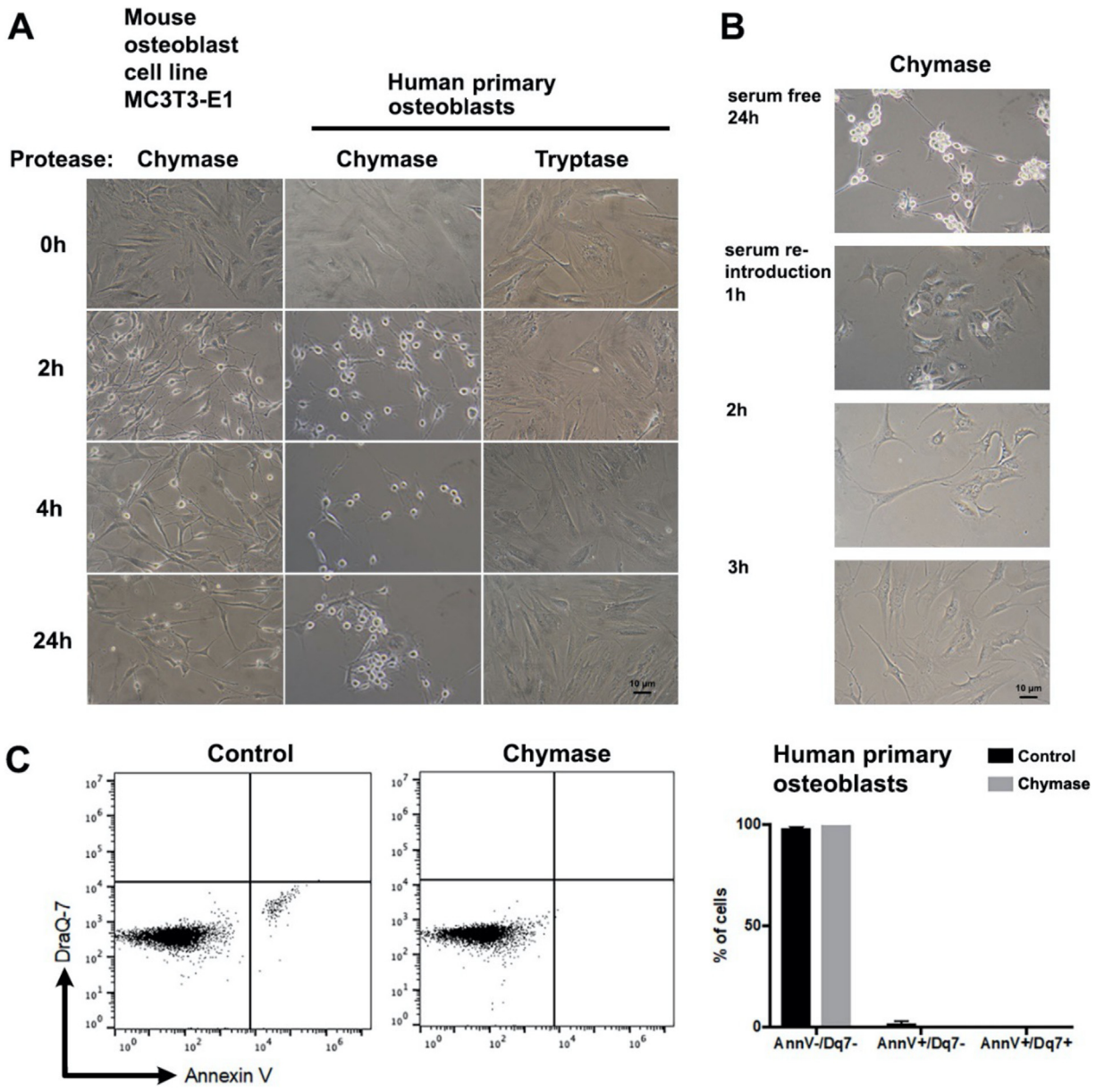

Fig. 1. Effect of mast cell proteases on human osteoblast morphology. Cultured human primary osteoblasts or a mouse osteoblast cell line (MC3T3-E1) were incubated with either human chymase (50 nM) or tryptase (50 nM) under serum-free conditions for the indicated time periods. **(A)** Light microscopy images of control (non-treated) and chymase-treated cells. **(B)** Human primary osteoblasts were incubated with human chymase (50 nM) for 24 h under serum-free conditions, followed by re-introduction of serum as indicated; note the reversal to normal morphology after re-introduction of serum. (**C)** Viability of untreated and chymase-treated (24 h, 50 nM) osteoblasts as assessed by flow cytometry after staining with Annexin V and DRAQ7: viable cells (Annexin V^-/DRAQ7$^-$), apoptotic cells (Annexin V^+/DRAQ7$^-$), and late apoptotic/necrotic cells (Annexin V^+/DRAQ7$^+$). Representative dot plots are shown to the left and quantification of data is shown to the right. Data represent means of triplicate determinations ±SEM.

in the absence or presence of heparin. These experiments revealed that the impact of chymase on the osteoblasts was delayed by the presence of heparin (Suppl. Fig. 3). Hence, these findings suggest that the impact of chymase on the osteoblasts is dependent on both its catalytic activity and on its positive charge.

Chymase causes extensive actin remodeling in primary human osteoblasts

To provide further insight into the morphological effects of chymase on osteoblasts, we performed confocal microscopy, using nuclear-, cell membrane- and actin markers. As expected, F-actin was

uniformly distributed within the cytoplasm of non-treated osteoblasts, forming abundant microfilaments (Fig. 2A-B). However, upon chymase treatment, disruption of the actin filaments was seen (Fig. 2B, white arrows in upper panels). Moreover, the actin distribution became more punctuated and a striking reorganization of actin to regions proximal to the nucleus was seen (Fig. 2,A-B). Fig. 2C depicts enlarged front- and side views of a representative osteoblast, highlighting the dramatic reorganization of actin to the nucleus-proximal regions in response to chymase treatment. Assessment of the osteoblasts by the cell-membrane probe revealed that chymase treatment caused the formation of clearly visible, thread-like cellular protrusions, which appeared to connect individual osteoblasts (Fig. 2B; white arrows in lower right panel).

Chymase affects the output of extracellular matrix compounds from osteoblasts

Osteoblasts are major producers of extracellular matrix (ECM) proteins such as collagen and fibronectin destined for deposition in the bone tissue. To address whether chymase can affect the output of such proteins, we first analyzed osteoblast-conditioned medium for the presence of collagen-1 and fibronectin. As seen in Fig. 3A, a distinct collagen-1 band was seen in medium collected from non-treated osteoblasts, confirming that the osteoblasts indeed secreted this protein. However, the collagen band was undetectable in medium collected from chymase-treated osteoblasts, indicating that chymase had the capacity to reduce the levels of collagen-1. Further, medium from non-treated cells also contained fibronectin, migrating as an expected ~250 kDa band under reducing conditions and as a high molecular weight band under nonreducing conditions (Fig. 3A). However, upon treatment of the osteoblasts with chymase, fibronectin was extensively degraded into fragments of ~90−110 kDa, suggesting that chymase had a strong capacity to execute proteolytic processing of fibronectin secreted by osteoblasts. As judged by Affymetrix transcriptomic analysis, chymase did not significantly affect the levels of mRNA coding for either fibronectin or collagen-1 (data not shown).

Previous studies have shown that chymase can either directly impact on various ECM proteins or, alternatively, activate matrix metallopeptidases (MMPs) that, in turn, may execute the actual proteolysis of such proteins [20, 22]. To assess whether chymase can activate MMPs secreted by osteoblasts, we conducted gelatin zymography analysis (detects gelatinases, in particular MMP2 and MMP9) of conditioned medium from non- and chymase-treated osteoblasts. This revealed the presence of a ~70 kDa gelatinolytic compound in osteoblast-conditioned medium, in agreement with the features of pro-MMP2 (Fig. 3B; see Suppl. Fig. 4 for a time course assessment). In the absence of chymase, only the non-processed form of MMP2 was seen. However, after treatment with chymase, also the active form of MMP2 was observed, indicating that chymase had the capacity to proteolytically activate pro-MMP2 secreted by human osteoblasts. In agreement with these observations, also the mouse osteoblast cell line (MC3T3-E1) secreted pro-MMP2, and chymase was found to cause activation of the pro-MMP2 to its active form (Fig. 3B).

Chymase affects intracellular signaling pathways in human osteoblasts

To approach the mechanism by which chymase affects the osteoblasts, we next considered the possibility that chymase might affect intracellular signaling pathways. To address this, we adopted a phosphorylation multi-pathway profiling array analysis in which effects on protein phosphorylation was analyzed after chymase addition to the osteoblasts. The array encompassed components of several signaling pathways, including the MAPK, AKT, JAK/STAT, NFκB and TGFβ pathways. Out of these, chymase affected most consistently the TGFβ family panel, as shown by a reduction of the phosphorylation of the TGFβ/BMP pathway proteins: SMAD2 (S245/250/255; inversely correlated to TGFβ activation, i.e., dephosphorylation causes activation [32]) and SMAD5 (S463/465). In addition, chymase affected the phosphorylation status of the members of the activator protein (AP)−1 family of transcription factors: ATF2 (T69/71), cFOS (T232) and cJUN (S73) (Fig. 4A-B). An effect of chymase on the TGFβ pathway was also supported by the induction of SMAD2 phosphorylation at the Ser465/467 site, representing a well-known activating modification [33] (Fig. 4G). Together, these findings suggest that chymase overall has an activating impact on TGFβ/BMP signaling in human osteoblasts.

The phosphorylation status of several of the proteins involved in AKT signaling was also affected (Fig. 4C), and several proteins involved in NFκB signaling were affected by chymase (Fig. 4D). Effects of chymase were also seen on the phosphorylation status of several of the proteins involved in the MAPK pathway (Fig. 4E), whereas the JAK/STAT pathway was less affected (Fig. 4F).

Chymase affects the transcriptome of human osteoblasts

To provide further insight into the mechanism by which mast cell chymase affects osteoblasts, we conducted a global transcriptome analysis based on the Affymetrix microarray platform. This revealed that chymase had extensive effects on the osteoblast transcriptome, including a significantly

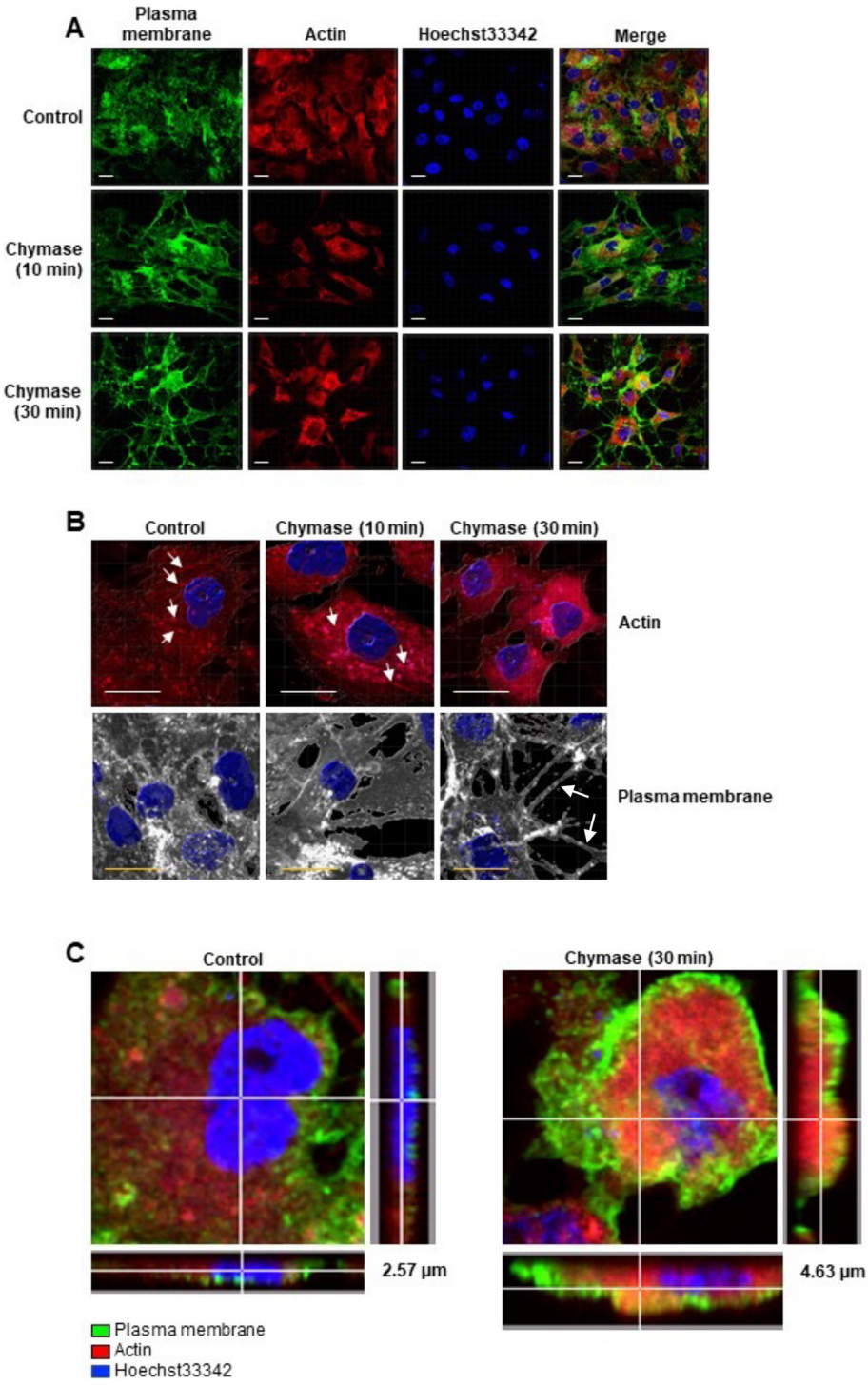

Fig. 2. Effect of mast cell chymase on actin- and membrane organization in human osteoblasts. (**A)** Human primary osteoblasts were incubated under serum-free conditions, either alone or in the presence of 50 nM chymase for the indicated time periods. Cells were then stained with a cell membrane probe (WGA-A488; green) and a probe for actin (ActinRed^{TM} 555; red). Nuclei were visualized with Hoechst 33342 (blue). Fluorescent staining of chymase treated osteoblasts on glass cover slides, showing membrane (green), actin (red) and nucleus (blue) staining. (**B)** 3-D front views generated from Z-stack sections showing the disruption of actin filaments (white arrows) in upper panels, followed by a dramatic contraction of the cells in lower panels. **(C)** Enlarged front and side view of a representative control (non-treated) and chymase-treated osteoblast, revealing a profound rounding up/thickening of the cell after chymase treatment. Scale bars, 10 μm.

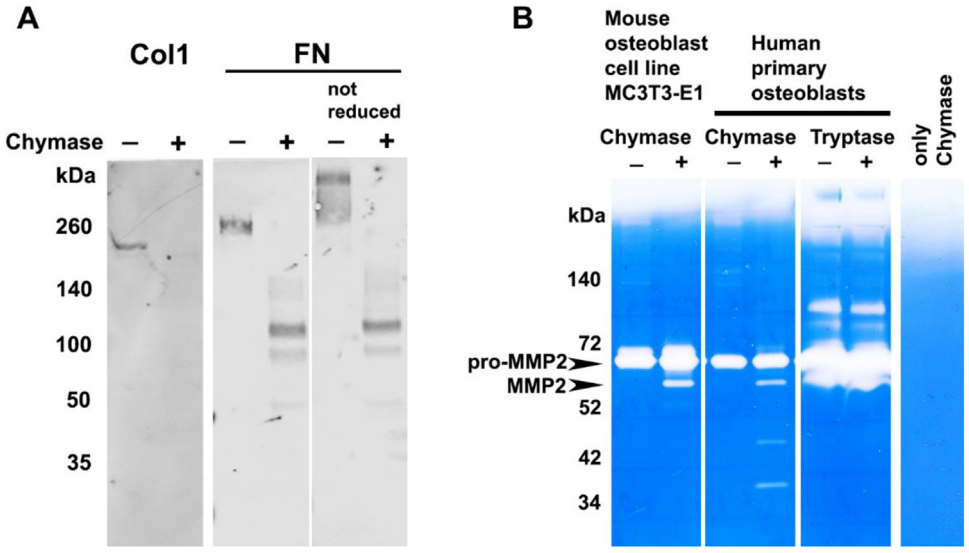

Fig. 3. Effect of mast cell proteases on collagen-1, fibronectin and matrix metallopeptidase-2 produced by osteoblasts. Primary human osteoblasts or a mouse osteoblast cell line (MC3T3-E1) were cultured under serum free conditions for 24 h, either in the absence or presence of chymase (50 nM) or tryptase (50 nM) as indicated. Conditioned medium was recovered from the cell cultures, and was **(A)** analyzed by Western blotting for collagen-1 (Col1) and fibronectin (FN), or **(B)** by gelatin zymography. In **(B)**, bands representing pro-MMP2 and active MMP2 are indicated. Shown are representative results from duplicate experiments; both experiments yielded similar results.

upregulated expression of 69 genes (Table 1), as well as significant down-regulation of 45 transcripts (Table 2).

To validate these findings, we conducted qPCR analysis of genes selected from this category, focusing on genes involved in the TGFβ pathway (TGFB1 and SMAD7), and genes associated with a bone-generating osteoblast phenotype [a disintegrin and metalloproteinase with thrombospondin motifs 1 (ADAMTS1)], connective tissue growth factor (CTGF/CCN2) and osteoprotegerin (TNFRSF11B/OPG)]. As shown in Fig. 5, the qPCR analysis indeed confirmed the upregulated expression of TGFB1 and SMAD7 in response to chymase, and the down-regulated expression of ADAMTS1, CTGF/CCN2 and TNFRSF11B/OPG was also confirmed.

Chymase affects the expression of TGFβ, OPG and CTGF at the protein level in osteoblasts

To further substantiate the observed effects of chymase on gene transcription in osteoblasts, we next chose to validate key findings by assessing effects on the corresponding proteins by using ELISA analysis. This analysis confirmed, at the protein level, that chymase induced TGFβ expression in osteoblasts (Fig. 6A). This was seen both in the cell lysates (intracellular TGFβ) and in the cell supernatant (released TGFβ). In agreement with the gene expression data, we also observed a consistent reduction in OPG protein expression after exposure of the osteoblasts to chymase (Fig. 6B). This was seen in the intracellular compartment at 24 h after chymase exposure, and extracellularly at 8 and 24 post chymase addition. However, at early time points after chymase addition (1 h), a significant increase in OPG levels was seen extracellularly (Fig. 6B). In agreement with the effects on CTGF gene expression, chymase induced a decrease in the levels of CTGF protein. This was seen intracellularly at 1 and 8 h after chymase addition (Fig. 6C).

Chymase binds to and is taken up by osteoblasts

As an additional approach to elucidate the mechanism by which chymase affects osteoblast functionality, we considered the possibility that chymase might interact with the cells.

To examine this, we labelled chymase with Alexa Fluor-488. Labelled chymase was then added to the osteoblasts, followed by confocal microscopy analysis. As seen in Fig. 7C, labelled chymase was recovered on the cell surface of the osteoblasts, indicating that chymase indeed can interact with the cells. Strikingly, chymase was also found within the cytoplasm of the osteoblasts, being frequently located in the vicinity of the cell nucleus (Fig. 7A-B). We also assessed the possibility that chymase may act via any of the various protease-activated receptors (PARs) that are present on many cell types [34]. However, agonists to either PAR1, PAR2, PAR3 or PAR4 did not replicate the effects seen after chymase treatment of the osteoblasts (Suppl. Fig. 5), suggesting that chymase affects the cells through

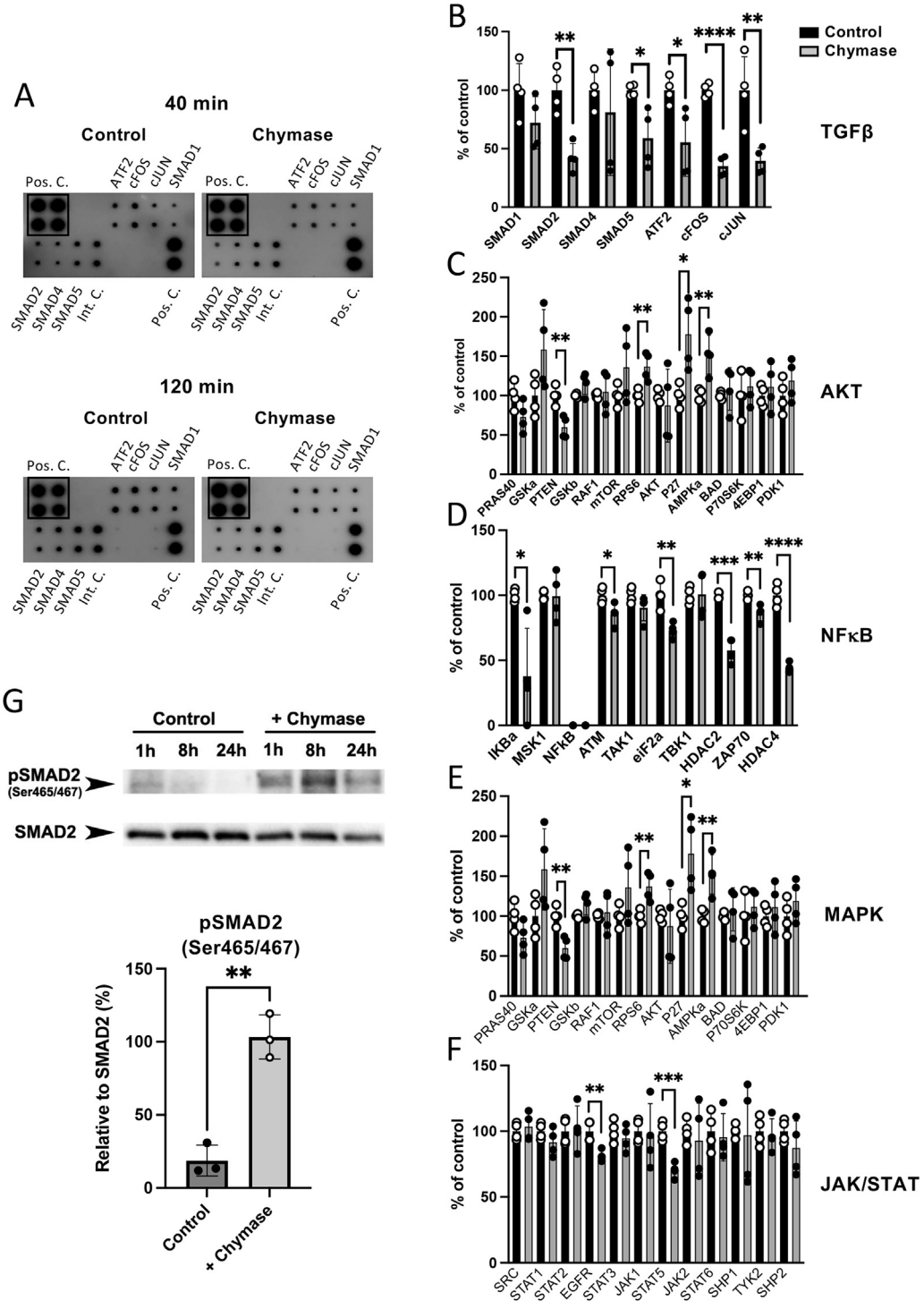

Fig. 4. Effect of chymase on signaling pathways in human osteoblasts. Primary human osteoblasts were incubated under serum-free conditions either in the absence or presence of chymase (50 nM) for the indicated time periods. Cells were recovered, and cell lysates were **(A)** analyzed by a phosphorylation multi-pathway profiling array. **(B-F)** Quantification of signal intensities representing phosphorylated proteins of the TGFβ **(B)**, AKT **(C)**, NFκB **(D)**, MAPK **(E)** and JAK/STAT **(F)** pathways. **(G)** Western blot analysis showing the effect of chymase on the phosphorylation of SMAD2 at the Ser465/467 site, using non-phosphorylated SMAD2 as house-keeping control. Quantification of band intensities is shown below. Data is given as mean values ±SD ($n = 3-4$). *, $p \leq 0.05$; **, $p \leq 0.01$; ***, $p \leq 0.001$; ****, $p \leq 0.0001$.

Table 1. Upregulated genes in human osteoblasts treated with chymase (24 h), grouped according to cell function.

Cell type/response	Symbol	Rank	log2change	avgintensity	adj p-value	Cytoband
Growth factor/secreted factor						
neuromedin B	NMB	4	3.850	10.452	0.004	15q22-qter
Norrie disease (pseudoglioma)	NDP	33	1.925	6.600	0.025	Xp11.4
transforming growth factor beta 1	TGFB1	38	2.643	10.701	0.028	19q13.1
frizzled-related protein	FRZB	55	1.650	5.599	0.029	2q32.1
chitinase 3-like 2	CHI3L2	83	2.350	10.733	0.046	1p13.3
family with sequence similarity 196, member A	INSYN2A	91	1.975	5.634	0.048	10q26.2
olfactomedin like 2B	OLFML2B	98	2.631	12.295	0.048	1q23.3
Lipid/polyamine metabolism						
fatty acid binding protein 5 (psoriasis-associated)	FABP5	9	2.717	7.778	0.014	8q21.13
perilipin 2	PLIN2	14	3.693	13.143	0.019	9p22.1
fatty acid binding protein 5 (psoriasis-associated)	FABP5	17	3.009	8.776	0.019	8q21.13
spermidine/spermine N1-acetyltransferase 1	SAT1	28	3.209	13.431	0.025	Xp22.1
mesenteric estrogen-dependent adipogenesis	MEDAG	95	1.291	16.050	0.048	13q12.3
Cell membrane/receptor/transporter						
endothelin receptor type A	EDNRA	10	5.098	10.699	0.019	4q31.22
chemokine (C—C motif) receptor 1	CCR1	18	2.101	5.845	0.019	3p21
interleukin 1 receptor, type I	IL1R1	30	2.241	13.731	0.025	2q12
EPH receptor B2	EPHB2	34	1.670	7.033	0.025	1p36.1-p35
frizzled class receptor 8	FZD8	37	3.296	9.413	0.028	10p11.21
sarcoglycan delta	SGCD	70	1.928	13.837	0.040	5q33-q34
transmembrane protein 233	TMEM233	71	1.627	7.188	0.040	12q24.23
integrin, alpha 2 (CD49B)	ITGA2	88	3.550	11.705	0.048	5q11.2
integrin alpha 10	ITGA10	106	1.678	7.705	0.049	1q21
solute carrier family 6, member 6	SLC6A6	107	1.795	13.961	0.049	3p25.1
transmembrane protein 38B	TMEM38B	110	1.643	9.941	0.049	9q31.2
Intracellular signaling						
GTP binding protein overexpressed in skeletal muscle	GEM	11	3.599	10.589	0.019	8q13-q21
regulator of G-protein signaling 2	RGS2	16	3.246	7.303	0.019	1q31
Rho GTPase activating protein 24	ARHGAP24	29	2.543	11.071	0.025	4q22.1
Rho GTPase activating protein 32	ARHGAP32	45	2.065	9.070	0.028	11q24.3
SMAD family member 7	SMAD7	72	2.141	9.694	0.041	18q21.1
sulfatase 2	SULF2	79	2.148	12.277	0.045	20q13.12
TBC1 domain family, member 15	TBC1D15	80	1.302	12.996	0.045	12q21.1
regulator of G-protein signaling 17	RGS17	92	1.571	6.834	0.048	6q25.3
inositol 1,4,5-trisphosphate receptor, type 1	ITPR1	97	2.859	9.589	0.048	3p26.1
folliculin interacting protein 2	FNIP2	104	2.127	11.705	0.049	4q32.1
MAM domain containing 2	MAMDC2	105	1.820	6.847	0.049	9q21.12
RAS, dexamethasone-induced 1	RASD1	109	2.168	6.389	0.049	17p11.2
amyloid beta precursor protein-binding, family B, 1, i.p.	APBB1IP	111	1.464	9.531	0.049	10p12.1
eukaryotic elongation factor 2 kinase	EEF2K	114	2.266	9.196	0.050	16p12.2
Nuclear/transcription						
sine oculis binding protein homolog	SOBP	12	2.532	8.509	0.019	6q21
hes family bHLH transcription factor 1	HES1	15	3.515	7.021	0.019	3q28-q29
SET domain and mariner transposase fusion gene	SETMAR	22	1.729	7.961	0.024	3p26.1
zinc finger protein 267	ZNF267	32	2.012	10.937	0.025	16p11.2
vestigial-like family member 4	VGLL4	43	2.578	9.303	0.028	3p25.3
TEA domain family member 2	TEAD2	52	2.032	8.154	0.029	19q13.3
family with sequence similarity 87, member B	FAM87B	56	1.941	8.359	0.029	1p36.33
HMG box domain containing 3	HMGXB3	63	1.372	9.820	0.038	5q32
chromodomain helicase DNA binding protein 4	CHD4	68	1.685	10.329	0.040	12p13
tumor protein p63 regulated 1	TPRG1	69	2.034	5.502	0.040	3q28
charged multivesicular body protein 1B	CHMP1B	73	1.479	13.130	0.044	18p11.21
snail family zinc finger 2	SNAI2	76	2.205	15.559	0.045	8q11
cysteine and glycine-rich protein 2	CSRP2	89	2.534	10.722	0.048	12q21.1
splicing factor proline/glutamine-rich	SFPQ	93	1.564	12.078	0.048	1p34.3
zinc finger, AN1-type domain 5	ZFAND5	94	1.485	14.707	0.048	9q13-q21
WD repeat domain 26	WDR26	99	1.515	13.284	0.048	1q42.13
TCDD-inducible poly(ADP-ribose) polymerase	TIPARP	112	1.401	10.458	0.049	3q25.31
Protease/inhibitor						
ADAM metallopeptidase domain 17	ADAM17	31	2.057	11.933	0.025	2p25

(*continued*)

Table 1 (*Continued*)

Cell type/response	Symbol	Rank	log2change	avgintensity	adj p-value	Cytoband
matrix metallopeptidase 14 (membrane-inserted)	MMP14	44	2.075	15.818	0.028	14q11.2
serine peptidase inhibitor, Kazal type 1	SPINK1	67	2.303	6.204	0.040	5q32
Ubiquitination						
ubiquitin-like 3	UBL3	35	1.667	16.130	0.025	13q12-q13
F-box protein 30	FBXO30	57	1.565	11.905	0.030	6q24
F-box and WD rep. dom. cont. 7, E3 ubiq. prot. lig.	FBXW7	62	2.342	10.063	0.035	4q31.3
F-box protein 32	FBXO32	90	2.200	13.365	0.048	8q24.13
Cytoskeletal/mitochondria/golgi						
myosin regulatory light chain interacting protein	MYLIP	36	1.649	10.078	0.025	6p22.3
aldo-keto reductase family 1, member B15	AKR1B15	42	3.136	9.242	0.028	7q33
midline 2	MID2	46	1.941	9.535	0.028	Xq22.3
coiled-coil domain containing 39	CCDC39	47	1.904	7.980	0.028	3q26.33
ST3 beta-galactoside alpha-2,3-sialyltransferase 1	ST3GAL1	53	1.539	8.709	0.029	8q24.22
aldo-keto reductase family 1, member B10	AKR1B10	54	2.680	7.758	0.029	7q33
peptidylprolyl isomerase F	PPIF	78	2.736	7.755	0.045	10q22.3
golgin A6 family-like 5, pseudogene	GOLGA6L5P	96	1.226	8.996	0.048	15q25.2

PAR-independent mechanisms. Together, these findings suggest that chymase is taken up into the osteoblasts, possibly exerting effects on osteoblasts through mechanisms operative within the intracellular compartment.

Discussion

Previous research has established a link between mast cells and bone homeostasis. For example, there is extensive evidence that expanded mast cell populations, i.e., mastocytosis, is frequently associated with osteoporosis and bone fractures [10–14]. Moreover, studies in animal models have revealed a correlation between mast cell numbers and the manifestations of various bone-degenerating pathologies [16–19]. Although these previous findings have suggested an impact of mast cells on bone homeostasis, it has not been certain by what mechanisms mast cells exert such effects. In a previous study, we provided a partial answer to this by showing that mice lacking mast cell chymase (Mcpt4$^{-/-}$) displayed an expanded bone mass, especially in the diaphyseal bone [26]. These findings suggest that chymase can have a negative impact on bone mass, and it is thus conceivable that the overall negative impact of mast cells on bone homeostasis can be mediated by mast cell chymase. However, although these findings implicate chymase in the regulation of bone mass, the exact underlying mechanism has not been elucidated, and it has not been known whether chymase can have a corresponding impact in a human setting.

One potential scenario could be that chymase suppresses bone mass by causing activation of osteoclasts, whereas another possibility could be that the negative impact of chymase on bone mass is caused by direct effects on osteoblast populations. In our previous study, the data indicated that the absence of chymase Mcpt4 affected osteoblast- but not osteoclast markers [26], which prompted us to investigate whether chymase can have a direct impact on osteoblasts.

Our data indeed reveal a major impact of mast cell chymase on human osteoblasts. Firstly, we noted that chymase had striking effects on the morphology of the osteoblast, causing a marked cellular contraction accompanied by extensive actin remodeling. In line with these effects, we noted that chymase affected the expression of DIAPH3, a major regulator of the actin cytoskeleton [35, 36]. Importantly, no corresponding effect was mediated by tryptase, another major mast cell protease, suggesting that the effects of chymase on osteoblasts represent chymase-specific events. Clearly, these findings suggest that chymase has a profound and specific effect on osteoblasts, and it is plausible that such events will affect the ability of the osteoblasts to participate in bone formation.

To address more directly the effect of chymase on the ability of osteoblasts to produce ECM compounds, we assessed effects of chymase on the output of collagen-1 and fibronectin from the cells. In line with a negative impact of chymase on the ability of the osteoblasts to produce bone-building ECM material, we noted that chymase caused a dramatic decrease in the levels of secreted collagen-1, as well as extensive degradation of secreted fibronectin. The degradation of osteoblast-produced fibronectin by chymase is in line with several previous studies in which fibronectin has been identified as a major substrate for mast cell chymase [37–39]. The reduction in collagen-1 could potentially be explained by direct collagenase activity. However,

Table 2. Downregulated genes in human osteoblasts treated with chymase (24 h), grouped according to cell function.

Cell type/response	Symbol	Rank	log2change	avgintensity	adj p-value	Cytoband
Protease/inhibitor						
ADAM metallopeptidase with thrombospondin type 1 motif 1	ADAMTS1	1	−4.825	12.945	0.001	21q21.2
carboxypeptidase A4	CPA4	25	−2.768	7.476	0.025	7q32
ADAM metallopeptidase with thrombospondin type 1 motif 5	ADAMTS5	50	−1.833	9.313	0.029	21q21.3
Cytoskeletal/mitochondria/golgi						
diaphanous-related formin 3	DIAPH3	2	−3.571	8.541	0.004	13q21.2
four and a half LIM domains 2	FHL2	20	−4.140	10.155	0.021	2q12.2
sphingomyelin synthase 2	SGMS2	21	−2.695	12.197	0.024	4q25
peptidylprolyl isomerase (cyclophilin)-like 1	PPIL1	41	−1.577	8.299	0.028	6p21.1
serine active site containing 1	SERAC1	51	−1.692	9.415	0.029	6q25.3
clathrin, light chain B	CLTB	103	−1.425	11.566	0.049	5q35
core 1 synthase, glycoprot-N-acetylgal 3-b-galactosyltransf 1	C1GALT1	108	−1.564	14.483	0.049	7p21.3
Intracellular signaling						
G protein-coupled receptor 1	GPR1	3	−3.465	10.175	0.004	2q33.3
dedicator of cytokinesis 5	DOCK5	48	−2.368	12.738	0.029	8p21.2
atypical chemokine receptor 3	ACKR3	58	−2.065	12.211	0.030	2q37.3
maternal embryonic leucine zipper kinase	MELK	64	−1.961	7.075	0.039	9p13.2
phospholipase C, epsilon 1	PLCE1	77	−2.658	8.663	0.045	10q23
dimethylarginine dimethylaminohydrolase 1	DDAH1	81	−3.192	12.371	0.046	1p22
Rho GTPase activating protein 18	ARHGAP18	86	−1.789	9.093	0.048	6q22.33
phospholipid phosphatase 3	PLPP3	102	−1.526	16.389	0.049	1p32.2
Cholesterol metabolism						
methylsterol monooxygenase 1	MSMO1	5	−2.988	15.383	0.013	4q32-q34
24-dehydrocholesterol reductase	DHCR24	19	−2.596	7.517	0.021	1p32.3
neutral cholesterol ester hydrolase 1	NCEH1	85	−1.952	8.861	0.048	3q26.31
Growth factor/secreted factor						
follistatin (TGF-β superfamily antagonist)	FST	6	−4.549	12.603	0.013	5q11.2
chemokine (C-X-C motif) ligand 6	CXCL6	13	−2.849	6.193	0.019	4q13.3
connective tissue growth factor	CTGF /CCN2	23	−6.061	10.507	0.025	6q23.1
chromosome 12 open reading frame 75 (Follistatin like)	FSTL1	26	−1.871	12.758	0.025	12q23.3
thrombospondin 1	THBS1	39	−3.687	15.869	0.028	15q15
cysteine-rich, angiogenic inducer, 61	CYR61/CCN1	61	−3.680	8.956	0.033	1p22.3
stanniocalcin 2	STC2	65	−3.690	11.277	0.039	5q35.1
dickkopf WNT signaling pathway inhibitor 1	DKK1	74	−5.710	9.792	0.045	10q11.2
tumor necrosis factor receptor superfamily, member 11b	TNFRSF11B	75	−4.298	11.348	0.045	8q24
chemokine (C-X-C motif) ligand 1	CXCL1	100	−2.570	6.771	0.049	4q21
Nuclear/transcription						
MIR4435−2 host gene	MIR4435−2HG	7	−4.155	10.095	0.013	2q13
long intergenic non-protein coding RNA 152	CYTOR	24	−4.201	11.340	0.025	2p11.2
spectrin repeat containing, nuclear envelope 1	SYNE1	27	−1.736	8.278	0.025	6q25
cell division cycle 6	CDC6	49	−2.342	7.076	0.029	17q21.3
oral cancer overexpressed 1	LTO1	59	−1.378	8.861	0.033	11q13.3
SHC SH2-domain binding protein 1	SHCBP1	60	−2.941	6.897	0.033	16q11.2
cyclin-dependent kinase 1	CDK1	66	−2.211	6.593	0.040	10q21.1
TTK protein kinase	TTK	82	−2.619	6.613	0.046	6q14.1
ribonucleotide reductase M2	RRM2	84	−3.626	7.200	0.048	2p25-p24
cyclin D1	CCND1	87	−1.446	16.136	0.048	11q13
centromere protein U	CENPU	101	−2.247	8.010	0.049	4q35.1
mohawk homeobox	MKX	113	−2.756	8.232	0.050	10p12.1
Cell membrane/receptor/transporter						
potassium channel, two pore domain subfamily K, member 2	KCNK2	8	−2.855	12.582	0.013	1q41
natriuretic peptide receptor 3	NPR3	40	−2.122	11.236	0.028	5p13.3

chymase has not hitherto been identified as a bona fide collagenase, and direct proteolytic activity of chymase on collagen is thus not likely. On the other hand, chymase has previously been shown to cause activation of several proteases of the MMP family [37, 40, 41], and an alternative explanation for the reduction in collagen-1 output in chymase-treated osteoblasts could hence be that chymase activates latent MMPs, resulting in generation of active proteases with collagenolytic activity. In line with the latter possibility, our results showed that chymase had the capacity to activate osteoblast-secreted pro-MMP2.

In order to gain further insight into the effects of chymase on osteoblasts, we also studied its impact on intracellular signaling pathways. These analyses revealed that chymase had a preferential impact on the TGFβ pathway. Firstly, chymase was shown to cause reduced phosphorylation of the TGFβ-specific factor SMAD2 at the Ser245/250/255 site. Notably, dephosphorylation at this site is an activating modification, serving to promote nuclear

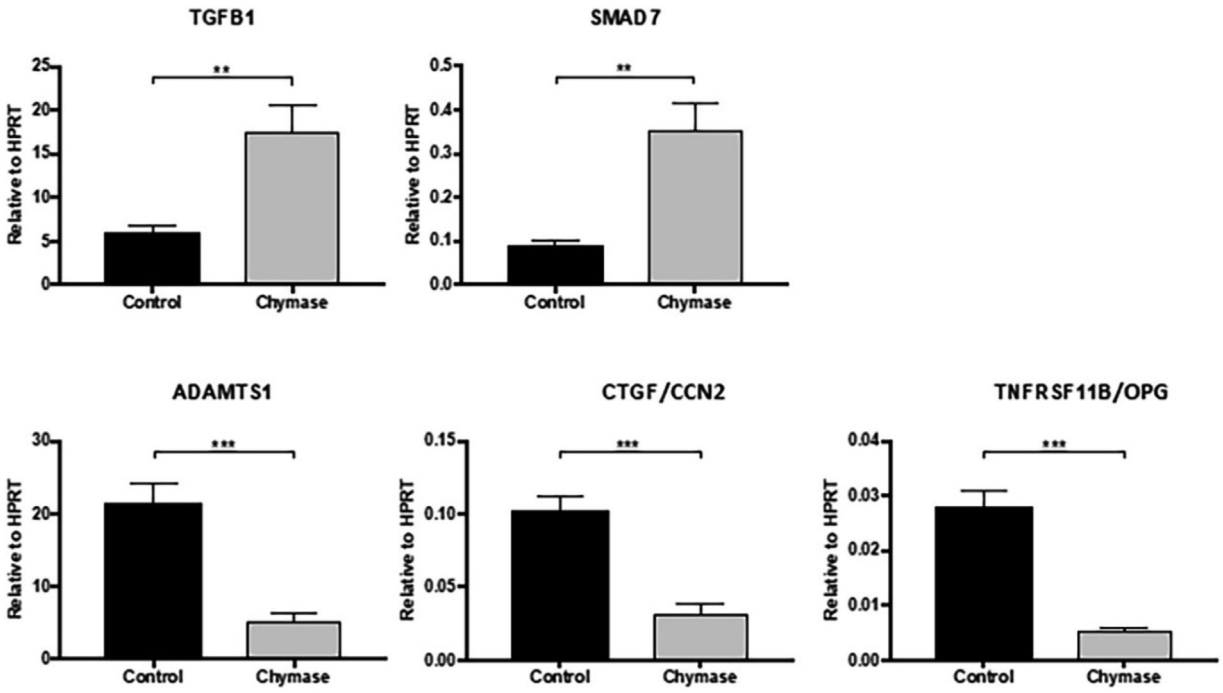

Fig. 5. Effect of chymase on the expression of the TGFB1, SMAD7, ADAMTS1, CTGF/CCN2 and TNFRSF11B/OPG genes in humas osteoblasts. Primary human osteoblasts were incubated under serum-free conditions in the absence (control) or presence of chymase (50 nM) for 24 h. Total RNA was purified from the cells and was analyzed by qPCR for content of mRNA representing the TGFB1, SMAD7, ADAMTS1, CTGF/CCN2 and TNFRSF11B/OPG genes as indicated. Data is given as mean values ±SEM ($n = 3$). **, $p \leq 0.01$; ***, $p \leq 0.001$.

translocation of SMAD2 in response to TGFβ [32]. A role for chymase in stimulating TGFβ signaling was also supported by a chymase-mediated increase in the phosphorylation of SMAD2 at the Ser465/467 site, representing an activating modification [33]. Further, extended treatment by chymase was also shown to promote dephosphorylation of SMAD1 and SMAD5, as well as a rapid increase of SMAD4 phosphorylation. Of these, SMAD4 is known to participate in both TGFβ and BMP signaling pathways [42] and has been linked to osteoblast function [43, 44]. In contrast, SMAD1 and SMAD5 are preferentially involved in BMP signaling [45], and our findings thus suggest that chymase may have a negative impact on signaling through BMP-mediated mechanisms. As further indications for a regulatory role of chymase on TGFβ and BMP signaling pathways, our transcriptome analysis revealed that chymase caused increased expression of the TGFβ target gene SMAD7 and reduced expression of the BMP target DKK1 [46]. Finally, our data show that chymase caused increased expression of TGFβ, both at the mRNA and protein level. We also noted that follistatin, a TGFβ superfamily antagonist, was one of the most downregulated genes after chymase treatment.

Collectively, our findings thus indicate that chymase has profound effects on TGFβ signaling events. Notably, TGFβ signaling has been implicated in the regulation of bone formation, but its net effect on bone may be complex and context-dependent. Although TGFβ is known to induce the expression of collagen and other compounds in osteoblasts, TGFβ signaling can also have a negative impact on bone building [47, 48]. Hence, effects on the TGFβ pathway are likely to affect bone remodeling events, but the net outcome of such effects may be multifaceted.

The exact mechanism behind the dramatic effect of chymase on osteoblast morphology is intriguing. However, it is known that TGFβ induces elongation of mouse osteoblasts and it is well-known that TGFβ expression is mechanosensitive and affected by cell shape [49, 50]. Hence, a plausible scenario is that the observed morphological effects were related to the induction of TGFβ signaling in the osteoblasts. Further, our transcriptome analysis revealed that chymase caused downregulation of KCNK2, a mechanosensitive potassium channel linked to anabolic effects of mechanical force on bone [51, 52]; we may thus speculate that effects on this gene may contribute to the observed effects of chymase on osteoblasts. In addition, our transcriptome analysis suggest that chymase causes de-differentiation of osteoblasts, as indicated by its respective effects on the expression of MIR4435−2HG [53], EDNRA [54], DKK1 [55], G protein-coupled receptor 1 (GPR1) [56], MSMO1 [57] and Neuromedin B [58]. Clearly,

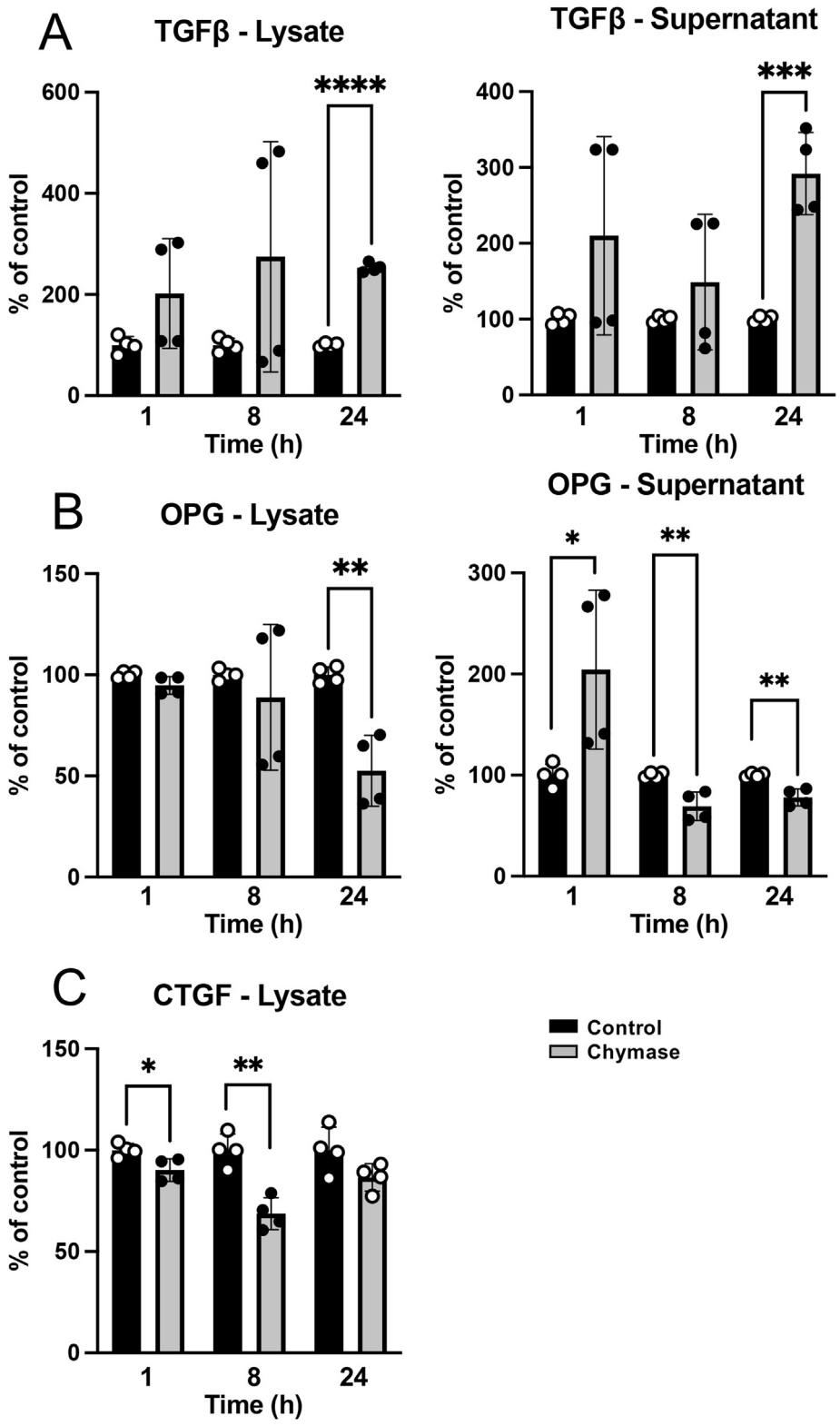

Fig. 6. Effect of chymase on the production and release of TGFβ, OPG and CTGF by human osteoblasts. Human primary osteoblasts were cultured under serum-free conditions, in the absence or presence of chymase (50 nM) for the indicated time periods. Cell pellets (lysates) and conditioned media (supernatant) were recovered and were analyzed by ELISA for content of **(A)** TGFβ, **(B)** osteoprotegerin (OPG) and **(C)** connective tissue growth factor (CTGF). Data is given as mean values ±SD ($n = 4$). *, $p \leq 0.05$; **, $p \leq 0.01$; ***, $p \leq 0.001$; ****, $p \leq 0.0001$.

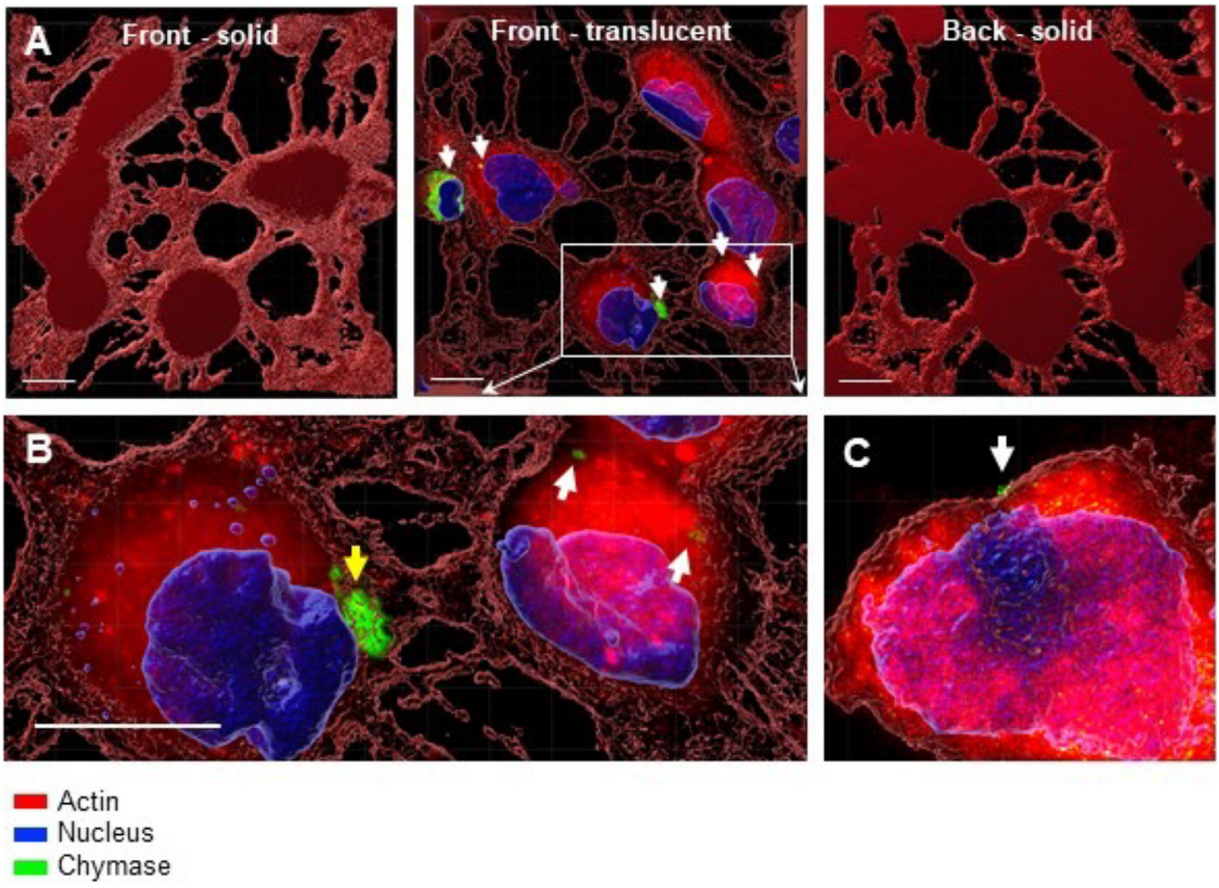

Fig. 7. Chymase interacts with and is taken up by human osteoblasts. Human primary osteoblasts were incubated under serum-free conditions, either alone or in the presence of Alexa Fluor-labeled chymase for 1 h. Cells were then stained with a probe for actin (ActinRed™ 555; red) and nuclei were visualized with Hoechst 33,342 (blue). (**A**) 3-D views generated from Z-stack sections. The central panel shows a translucent depiction of actin staining. Note the abundant chymase staining (green) in the cytoplasm (white arrows, central panel). The left and right panels show solid front and back views from the central panel; note the suppression of chymase staining in the solid views, indicating the intracellular localization of chymase. (**B**) Higher magnification of the area selected at central panel in A. Arrows show the cytoplasmatic localization of chymase. Note also the chymase staining close to the cell ucleus (yellow arrow). (**C**) Chymase staining of the cell surface (white arrow). Scale bars, 10 μm.

the observed negative impact of chymase on the various features of osteoblasts could thus be a reflection of a de-differentiation process.

As judged by the transcriptome analysis, the most significantly affected gene after chymase treatment of human osteoblasts was ADAMTS1, which was profoundly downregulated. This is in line with previous work where it has been shown that TGFβ has a negative effect on ADAMTS1 transcription [59, 60]. We have previously shown that ADAMTS1 is induced during osteogenesis in vitro [61] and it has also been demonstrated that ADAMTS1 was highly upregulated in rat bones after treatment with bone-anabolic PTH [62], altogether suggesting an important role for ADAMTS1 in bone formation. Further, it is notable that chymase caused an upregulated expression of FABP5, a gene which is implicated to have a negative impact on bone building [62]. Altogether, these findings add to the notion that chymase has an overall negative impact on osteoblast function.

In addition to its effects on TGFβ signaling compounds, we also demonstrated that chymase had a down-regulatory effect on OPG gene expression and protein output. OPG is a key factor produced by osteoblasts to regulate osteoclast formation, and it was recently shown that only OPG produced by osteoblasts has the capacity to affect bone remodeling, thereby emphasizing that osteoblasts are the major controllers of bone resorption [63, 64]. Hence, chymase-mediated suppression of OPG expression may lead to decreased bone-building capacity of the osteoblasts. Further, OPG has a negative impact on osteoclastogenesis, and the reduced OPG expression following chymase treatment may thus lead to both reduced osteoblast function and to an increase

in the generation of bone-degrading osteoclasts. Possibly, such a scenario could be linked to the increased bone resorption frequently seen in mastocytosis patients [10–14].

In summary, this study provides mechanistic insight into how mast cell chymase can have an impact on bone-building processes, here manifested by a profound impact on human osteoblasts. Based on this study and our previous findings in mice [26], chymase emerges as a potential drug target in settings characterized by bone loss. Notably, our findings suggest that chymase can act by interfering with osteoblast function, potentially reducing their rate of bone formation. Accordingly, interference with chymase would therefore represent an anabolic function, which currently is considered as the preferred strategy for improving bone strength [2, 3].

Experimental procedures

Reagents

Recombinant human chymase (C8118–50UG) was from Sigma-Aldrich, and was diluted in serum-free MEMα before applying to the cell cultures; buffer control experiments revealed that the vehicle for chymase (0.1% glycerol) had no impact on the osteoblast cultures (data not shown). Recombinant human skin β-tryptase was from Promega (Madison, WI), chymostatin from Santa Cruz Biotechnology (Dallas, TX) and pig mucosal heparin was purchased from Sigma-Aldrich. Annexin-V-FITC was from BD bioscience (Jan Jose, CA). DRAQ7™ was from Biostatus (Shepshed, UK). ActinRed™ 555, NucBlue™ Hoechst33342, wheat germ agglutinin-A488 and SlowFade™ diamond antifade mountant were from Invitrogen (Oregon, OR). Agonists for Protease-activated receptor PAR1 (AS-62937; AnaSpec, Fremont, CA), PAR2 (AC-55541; Tocris biosciences, Abingdon, UK), PAR3 (AS-62938, AnaSpec) and PAR4 (AS-60218–1; AnaSpec) were from the indicated sources.

Cell culture

Primary human osteoblasts were isolated from bone obtained from female donors undergoing knee replacement surgery and had no reported bone-related pathologies other than osteoarthritis. The osteoblastic phenotype of cells was verified by use of biochemical markers as previously described [65]. Uppsala University Hospital ethics committee approved this study (Permit Number: Dnr Ups 03–561) and waived the need for consent from these de-identified donors. The primary human osteoblasts and the mouse preosteoblast cell line, MC3T3-E1 subclone 4 (from ATCC) were cultured in MEMα GlutaMAX (ThermoFisher) supplemented with 10% heat inactivated foetal bovine serum, 100 mg/ml streptomycin and 100 U/ml penicillin. Change of media was done every 2nd or 3rd day.

Flow cytometry

Human osteoblasts were left untreated or treated with 50 nM of recombinant human chymase for 24 h. Cell were harvested using trypsin, washed once with PBS and pellets resuspended with Annexin binding buffer (Invitrogen). Annexin-V-FITC and DRAQ7 were added to each sample following manufacturer's recommendations. Cells were analyzed using BD Accuri flow cytometer and FlowJo software (BD bioscience).

Immunofluorescent staining of osteoblasts

Human osteoblasts were plated on 8-well chamber slides (Falcon, New York, NY) and were left untreated or treated with chymase. After treatment, cells were fixed in 4% PFA and plasma membrane was stained using wheat germ agglutinin-A488, followed by permeabilization with 1% BSA/0.1% Triton-X100/PBS and blocked in 3% BSA/0.1% Tween-20/PBS. Cells were probed with ActinRed™ 555 diluted in PBS and NucBlue™ Hoechst33342 according to manufacturer's recommendations. Next, cells were washed three times with PBS, mounted with SlowFade™ Diamond Antifade Mountant. Cells were analyzed using a laser-scanning macroscope equipped with ZEN 2009 software (LSM 710; Carl Zeiss, Berlin, Germany). Z-stack sections were analyzed using Imaris software from Bitplane (Zurich, Switzerland).

Assessment of the interaction of chymase with osteoblasts

Recombinant Human Chymase/CMA1 Protein (4099-SE-010, R&D systems) was labeled with the Alexa Fluor™ 488 Protein Labeling Kit (A10235, Thermo Fisher) according to the manufacturer's protocol except for the labeling step. Due to the limited protein amount, 50 μL of 1 M bicarbonate solution was added to 71 μL of the protein solution (0.14 mg/mL). The remaining protein purification steps were accomplished according to instructions provided by the manufacturer.

Osteoblasts were cultivated to 80% density on glass chamber slides, treated for 1 h with 12 nM unlabeled chymase + Alexa-488-labelled chymase, fixed in 4% PFA and permeabilized in ice-cold methanol. Cells were probed with ActinRed™ 555 diluted in PBS and NucBlue™ Hoechst33342 according to the manufacturer's recommendations. Next, cells were washed three times with PBS and mounted with SlowFade™ Diamond Antifade Mountant. Cells

were analyzed using a laser-scanning microscope equipped with ZEN 2009 software (LSM 710; Carl Zeiss, Berlin, Germany). Z-stack sections were acquired using 63x NA 1.40 oil objective and Imaris software from Bitplane (Zurich, Switzerland) was used to generate three dimensional-images with nuclear staining represented as solid block and actin staining in both translucent and solid block views. Front and back views of each image were also generated to confirm the intracellular localization of chymase staining.

Immunoblotting

Cells were lysed in 2x SDS Laemmli sample buffer (5% SDS, 25% glycerol, 150 mM Tris−HCl pH 6.8, 0.01% bromophenol blue, 100mMdithiothreitol (DTT)), boiled for 5 min and DNA was sheared with a 21 G needle followed by protein determination using the BCA protein reagent (Pierce, Rockford, IL). An equal amount of protein was separated by SDS-PAGE as described previously [66]. The primary antibody was detected with a horseradish peroxidase conjugated secondary antibody (DAKO, Denmark), which was diluted 1:20,000 and then processed by chemiluminescence with ECL reagents (Millipore, Billerica, MA). The pixel density of the bands was assessed using ImageJ software (U.S. National Institutes of Health, Bethesda, MD). Antibodies against the following were used: collagen pro-α1(I) C-telopeptide (LF-67, gift from Dr. Larry Fisher (NIDCR, National Institutes of Health) [67], fibronectin (kind gift from Dr. Staffan Johansson, Uppsala University), phospho-Ser465/467-SMAD2 (produced in house) and SMAD2/3 (#610,843, BD Transduction Laboratories).

Protein analysis

For an overview analysis of intracellular signaling pathways, the Human Phosphorylation Multi-pathway Profiling Array C55 (cat. # AAH-PPP-1−4, RayBio) was used according to the manufacturer's instructions. Commercially available ELISA kits were utilized for measurement of TGFβ1 (transforming growth factor beta 1, #DB100B, R&D Systems), TNFRSF11B/OPG (TNF receptor superfamily member 11b/osteoprotegerin, #E04692h, Cusabio) and CTGF/CCN2 (connective tissue growth factor/cellular communication network factor 2, #E07875h, Cusabio) according to the manufacturer's instructions.

RNA isolation

Total RNA extraction with TRI Reagent as described previously [66]. Isolated RNA was quantified using spectrophotometry by measuring the absorbance at 260 nm, and the 260/280 nm ratio was calculated. This ratio was 1.9−2.0 in all samples, indicating the absence of protein contamination. The integrity of sample RNAs was confirmed by capillary electrophoresis separating 18 S and 28 S ribosomal RNA on an Agilent Technologies (Palo Alto, CA) 2100 Bioanalyzer.

Microarray expression analysis

Two hundred ng of total RNA from each of 8 human osteoblast samples were used to generate amplified and biotinylated sense-strand cDNA from the entire expressed genome according to the GeneChip™ WT PLUS Reagent Kit User Manual (P/N 703174, Thermo Fisher Scientific Inc., Life Technologies, Carlsbad, CA 92008). GeneChip™ ST Arrays (GeneChip™ Clariom D Human Array) were hybridized for 16 h in a 45 °C incubator, rotated at 60 rpm. According to the GeneChip® Expression Wash, Stain and Scan Manual (P/N 702731, ThermoFisher Scientific Inc., Life Technologies, Carlsbad, CA) the arrays were then washed and stained using the Fluidics Station 450 and finally scanned using the GeneChip® Scanner 3000 7 G.

Microarray data analysis

Analysis of the gene expression data was carried out in the freely available statistical computing language R (http://www.r-project.org) using packages available from the Bioconductor project (www.bioconductor.org). The raw data was normalized using the robust multi-array average (RMA) method first suggested by Li and Wong in 2001 [68], see also [69]. In order to search for differentially expressed genes between the two groups of samples, an empirical Bayes moderated *t*-test was applied [70], using the 'limma' package [71]. To address the problem of multiple testing, the p-values were adjusted using the method of Benjamini and Hochberg [72]. An analysis of the functional annotation of the identified genes was performed using the Database for Annotation, Visualization and Integrated Discovery (DAVID) [73, 74].

Quantitative RT-PCR

Four hundred ng of total RNA was transcribed to cDNA using the TaqMan system (Applied Biosystems). Quantitative real time PCR (qPCR) was performed using inventoried TaqMan Gene Expression Assays for; TGFβ1 (transforming growth factor beta 1) ENSG00000105329 (Hs00998133_m1); SMAD7 (SMAD family member 7) ENSG00000101665 (Hs00998193_m1); ADAMTS1 (A disintegrin and metalloproteinase with thrombospondin motifs 1) ENSG00000154734 (Hs00199608_m1); CTGF/CCN2 (connective tissue growth factor/cellular communication network factor 2) ENSG00000118523

(Hs00854264_s1) and TNFRSF11B/OPG (TNF receptor superfamily member 11b/osteoprotegerin) ENSG00000164761 (Hs00900358_m1) according to the manufacturer's protocol, on a CFX96 Touch™ Real-Time PCR Detection System apparatus. Cycling protocol: 50 °C for 2 min, followed by 95 °C for 10 min and then 40 cycles of 95 °C 15 s followed by 60 °C for 1 min. For standardization, expression levels were divided by expression level for HPRT1 (hypoxanthine phosphoribosyltransferase 1) ENSG00000165704 (Hs02800695_m1), derived from dilution standard curves of Ct values for each gene. Each experiment was performed at least two times using triplicates.

Statistical analyses

The data (except the microarray analysis, described above) were analyzed by the Student's *t*-test or, for variables with deviations from the normal distribution, the Mann-Whitney U test. In every case, $p < 0.05$ was considered statistically significant.

Availability of data and material

The data that support the findings of this study are available within the article. Data and material will be made available on reasonable request to the corresponding author.

Funding

This study was funded by grants from the Swedish Research Council (GP, HM), The Swedish Cancer Foundation (GP), The Swedish Heart and Lung Foundation (GP) and The Knut and Alice Wallenberg Foundation (GP).

Author's contributions

TL conceptualization, data curation, formal analysis, investigation, resources, visualization, writing-original draft, writing review & editing; FM data curation, formal analysis, investigation, methodology, visualization, writing-review & editing; AS formal analysis, writing-review & editing; XZ formal analysis, writing review & editing; AMG formal analysis, visualization, writing review & editing; AM methodology, writing-review & editing; HM funding acquisition, methodology, writing-review & editing; GP conceptualization, funding acquisition, project administration, resources, writing original draft, writing review & editing.

Declaration of Competing Interest

The authors have no conflicts of interest to declare.

Acknowledgments

We would like to thank Elin Carlsson for excellent technical assistance.

Supplementary materials

Supplementary material associated with this article can be found, in the online version, at doi:10.1016/j.matbio.2022.07.005.

Received 21 January 2022;
Received in revised form 7 July 2022;
Accepted 26 July 2022
Available online 29 July 2022

Abbreviations:
MMP, matrix metallopeptidase; ADAMTS, ADAM metallopeptidase with thrombospondin type 1 motif; CTGF, connective tissue growth factor; OPG, osteoprotegerin; PTH, parathyroid hormone; ECM, extracellular matrix

Present address: Uppsala University, Department of Pharmaceutical Biosciences, Uppsala, Sweden

References

[1] E. Hernlund, A. Svedbom, M. Ivergard, J. Compston, C. Cooper, J. Stenmark, E.V. McCloskey, B. Jonsson, J.A. Kanis, Osteoporosis in the European Union: medical management, epidemiology and economic burden. A report prepared in collaboration with the International Osteoporosis Foundation (IOF) and the European Federation of Pharmaceutical Industry Associations (EFPIA), Arch. Osteoporos. 8 (2013) 136.
[2] S. Khosla, Increasing options for the treatment of osteoporosis, N. Engl. J. Med. 361 (8) (2009) 818–820.
[3] T.L. Jarvinen, K. Michaelsson, P. Aspenberg, H. Sievanen, Osteoporosis: the emperor has no clothes, J. Intern. Med. 277 (6) (2015) 662–673.
[4] S.J. Galli, J. Kalesnikoff, M.A. Grimbaldeston, A.M. Piliponsky, C.M. Williams, M. Tsai, Mast cells as "tunable" effector and immunoregulatory cells: recent advances, Annu. Rev. Immunol. 23 (2005) 749–786.
[5] D. Voehringer, Protective and pathological roles of mast cells and basophils, Nat. Rev. Immunol. 13 (5) (2013) 362–375.
[6] S.J. Galli, M. Tsai, T. Marichal, E. Tchougounova, L.L. Reber, G. Pejler, Approaches for analyzing the roles of mast cells and their proteases in vivo, Adv. Immunol. 126 (2015) 45–127.

[7] P. Bradding, G. Pejler, The controversial role of mast cells in fibrosis, Immunol. Rev. 282 (1) (2018) 198–231.
[8] B. Frame, R.K. Nixon, Bone-marrow mast cells in osteoporosis of aging, N. Engl. J. Med. 279 (12) (1968) 626–630.
[9] R.T. Turner, U.T. Iwaniec, K. Marley, J.D. Sibonga, The role of mast cells in parathyroid bone disease, J. Bone Miner. Res. 25 (7) (2010) 1637–1649.
[10] E. van der Veer, W. van der Goot, J.G. de Monchy, H.C. Kluin-Nelemans, J.J. van Doormaal, High prevalence of fractures and osteoporosis in patients with indolent systemic mastocytosis, Allergy 67 (3) (2012) 431–438.
[11] S. Seitz, F. Barvencik, T. Koehne, M. Priemel, P. Pogoda, J. Semler, H. Minne, M. Pfeiffer, J. Zustin, K. Puschel, C. Eulenburg, T. Schinke, M. Amling, Increased osteoblast and osteoclast indices in individuals with systemic mastocytosis, Osteoporos. Int. 24 (8) (2013) 2325–2334.
[12] N. Guillaume, J. Desoutter, O. Chandesris, L. Merlusca, I. Henry, S. Georgin-Lavialle, S. Barete, I. Hirsch, D. Bouredji, B. Royer, B. Gruson, C. Lok, H. Sevestre, R. Mentaverri, M. Brazier, J. Meynier, O. Hermine, J.P. Marolleau, S. Kamel, G. Damaj, Bone complications of mastocytosis: a link between clinical and biological characteristics, Am. J. Med. 126 (1) (2013) 75 e1-7.
[13] F.M. Ulivieri, L. Rinaudo, L.P. Piodi, V. Barbieri, G. Marotta, M. Sciume, F.I. Grifoni, B.M. Cesana, Usefulness of Dual X-ray Absorptiometry-Derived Bone Geometry and Structural Indexes in Mastocytosis, Calcif. Tissue Int. 107 (6) (2020) 551–558.
[14] M. Rossini, R. Zanotti, P. Bonadonna, A. Artuso, B. Caruso, D. Schena, D. Vecchiato, M. Bonifacio, O. Viapiana, D. Gatti, G. Senna, A. Riccio, G. Passalacqua, G. Pizzolo, S. Adami, Bone mineral density, bone turnover markers and fractures in patients with indolent systemic mastocytosis, Bone 49 (4) (2011) 880–885.
[15] B. Bouvard, F. Pascaretti-Grizon, E. Legrand, C. Lavigne, M. Audran, D. Chappard, Bone lesions in systemic mastocytosis: bone histomorphometry and histopathological mechanisms, Morphologie 104 (345) (2020) 97–108.
[16] B. Hassan, I. Fouilloux, B. Baroukh, A. Llorens, M. Biosse Duplan, M. Gosset, M. Cherruau, J.L. Saffar, Coordination of early cellular reactions during activation of bone resorption in the rat mandible periosteum: an immunohistochemical study, Heliyon 3 (10) (2017) e00430.
[17] P. Lesclous, D. Guez, A. Llorens, J.L. Saffar, Time-course of mast cell accumulation in rat bone marrow after ovariectomy, Calcif. Tissue Int. 68 (5) (2001) 297–303.
[18] T.A. Brennan, C.M. Lindborg, C.R. Bergbauer, H. Wang, F.S. Kaplan, R.J. Pignolo, Mast cell inhibition as a therapeutic approach in fibrodysplasia ossificans progressiva (FOP), Bone 109 (2018) 259–266.
[19] L. Zhang, T. Wang, M. Chang, C. Kaiser, J.D. Kim, T. Wu, X. Cao, X. Zhang, E.M. Schwarz, Teriparatide Treatment Improves Bone Defect Healing Via Anabolic Effects on New Bone Formation and Non-Anabolic Effects on Inhibition of Mast Cells in a Murine Cranial Window Model, J. Bone Miner. Res. 32 (9) (2017) 1870–1883.
[20] G. Pejler, M. Abrink, M. Ringvall, S. Wernersson, Mast cell proteases, Adv. Immunol. 95 (2007) 167–255.
[21] G. Pejler, S.D. Knight, F. Henningsson, S. Wernersson, Novel insights into the biological function of mast cell carboxypeptidase A, Trends Immunol. 30 (8) (2009) 401–408.
[22] S. Wernersson, G. Pejler, Mast cell secretory granules: armed for battle, Nat. Rev. Immunol. 14 (7) (2014) 478–494.
[23] L.B. Schwartz, A.M. Irani, K. Roller, M.C. Castells, N.M. Schechter, Quantitation of histamine, tryptase, and chymase in dispersed human T and TC mast cells, J. Immunol. 138 (8) (1987) 2611–2615.
[24] L.B. Schwartz, C. Riedel, J.P. Caulfield, S.I. Wasserman, K.F. Austen, Cell association of complexes of chymase, heparin proteoglycan, and protein after degranulation by rat mast cells, J. Immunol. 126 (6) (1981) 2071–2078.
[25] G. Pejler, Novel insight into the in vivo function of mast cell chymase: lessons from knockouts and inhibitors, J. Innate Immun. 12 (5) (2020) 357–372.
[26] T. Lind, A.M. Gustafson, G. Calounova, L. Hu, A. Rasmusson, K.B. Jonsson, S. Wernersson, M. Abrink, G. Andersson, S. Larsson, H. Melhus, G. Pejler, Increased bone mass in female mice lacking mast cell chymase, PLoS ONE 11 (12) (2016) e0167964.
[27] E. Mackey, S. Ayyadurai, C.S. Pohl, D.C.S, Y. Li, A.J. Moeser, Sexual dimorphism in the mast cell transcriptome and the pathophysiological responses to immunological and psychological stress, Biol Sex Differ 7 (2016) 60.
[28] G. Pejler, L. Berg, Regulation of rat mast cell protease 1 activity. Protease inhibition is prevented by heparin proteoglycan, Eur. J. Biochem. 233 (1) (1995) 192–199.
[29] W.W. Raymond, S. Su, A. Makarova, T.M. Wilson, M.C. Carter, D.D. Metcalfe, G.H. Caughey, Alpha 2-macroglobulin capture allows detection of mast cell chymase in serum and creates a reservoir of angiotensin II-generating activity, J. Immunol. 182 (9) (2009) 5770–5777.
[30] N.M. Schechter, J.L. Sprows, O.L. Schoenberger, G.S. Lazarus, B.S. Cooperman, H. Rubin, Reaction of human skin chymotrypsin-like proteinase chymase with plasma proteinase inhibitors, J. Biol. Chem. 264 (35) (1989) 21308–21315.
[31] E. Forsberg, G. Pejler, M. Ringvall, C. Lunderius, B. Tomasini-Johansson, M. Kusche-Gullberg, I. Eriksson, J. Ledin, L. Hellman, L. Kjellen, Abnormal mast cells in mice deficient in a heparin-synthesizing enzyme, Nature 400 (6746) (1999) 773–776.
[32] M. Kretzschmar, J. Doody, I. Timokhina, J. Massague, A mechanism of repression of TGFbeta/Smad signaling by oncogenic Ras, Genes Dev. 13 (7) (1999) 804–816.
[33] C.S. Hill, Transcriptional control by the SMADs, Cold Spring Harb. Perspect. Biol. 8 (10) (2016).
[34] D.M. Heuberger, R.A. Schuepbach, Protease-activated receptors (PARs): mechanisms of action and potential therapeutic modulators in PAR-driven inflammatory diseases, Thromb. J. 17 (2019) 4.
[35] S. Watanabe, T. De Zan, T. Ishizaki, S. Yasuda, H. Kamijo, D. Yamada, T. Aoki, H. Kiyonari, H. Kaneko, R. Shimizu, M. Yamamoto, G. Goshima, S. Narumiya, Loss of a Rho-regulated actin nucleator, mDia2, impairs cytokinesis during mouse fetal erythropoiesis, Cell Rep. 5 (4) (2013) 926–932.
[36] M.K. Rana, F.M. Aloisio, C. Choi, D.L. Barber, Formin-dependent TGF-beta signaling for epithelial to mesenchymal transition, Mol. Biol. Cell 29 (12) (2018) 1465–1475.
[37] E. Tchougounova, A. Lundequist, I. Fajardo, J.O. Winberg, M. Abrink, G. Pejler, A key role for mast cell chymase in the activation of pro-matrix metalloprotease-9 and pro-matrix metalloprotease-2, J. Biol. Chem. 280 (10) (2005) 9291–9296.
[38] E. Tchougounova, G. Pejler, M. Åbrink, The chymase, mouse mast cell protease 4, constitutes the major chymotrypsin-like activity in peritoneum and ear tissue. A role for mouse mast cell protease 4 in thrombin regulation and fibronectin turnover, J. Exp. Med. 198 (3) (2003) 423–431.

[39] T. Vartio, H. Seppa, A. Vaheri, Susceptibility of soluble and matrix fibronectins to degradation by tissue proteinases, mast cell chymase and cathepsin G, J. Biol. Chem. 256 (1) (1981) 471–477.
[40] K.C. Fang, W.W. Raymond, S.C. Lazarus, G.H. Caughey, Dog mastocytoma cells secrete a 92-kD gelatinase activated extracellularly by mast cell chymase, J. Clin. Invest. 97 (7) (1996) 1589–1596.
[41] J. Saarinen, N. Kalkkinen, H.G. Welgus, P.T. Kovanen, Activation of human interstitial procollagenase through direct cleavage of the Leu83-Thr84 bond by mast cell chymase, J. Biol. Chem. 269 (27) (1994) 18134–18140.
[42] H. Demagny, T. Araki, E.M. De Robertis, The tumor suppressor Smad4/DPC4 is regulated by phosphorylations that integrate FGF, Wnt, and TGF-beta signaling, Cell Rep. 9 (2) (2014) 688–700.
[43] V.S. Salazar, N. Zarkadis, L. Huang, J. Norris, S.K. Grimston, G. Mbalaviele, R. Civitelli, Embryonic ablation of osteoblast Smad4 interrupts matrix synthesis in response to canonical Wnt signaling and causes an osteogenesis-imperfecta-like phenotype, J. Cell Sci. 126 (Pt 21) (2013) 4974–4984.
[44] J.S. Park, M. Kim, N.J. Song, J.H. Kim, D. Seo, J.H. Lee, S.M. Jung, J.Y. Lee, J. Lee, Y.S. Lee, K.W. Park, S.H. Park, A reciprocal role of the Smad4-Taz axis in osteogenesis and adipogenesis of mesenchymal stem cells, Stem Cells 37 (3) (2019) 368–381.
[45] R. Nishimura, Y. Kato, D. Chen, S.E. Harris, G.R. Mundy, T. Yoneda, Smad5 and DPC4 are key molecules in mediating BMP-2-induced osteoblastic differentiation of the pluripotent mesenchymal precursor cell line C2C12, J. Biol. Chem. 273 (4) (1998) 1872–1879.
[46] N. Kamiya, T. Kobayashi, Y. Mochida, P.B. Yu, M. Yamauchi, H.M. Kronenberg, Y. Mishina, Wnt inhibitors Dkk1 and Sost are downstream targets of BMP signaling through the type IA receptor (BMPRIA) in osteoblasts, J. Bone Miner. Res. 25 (2) (2010) 200–210.
[47] K.S. Mohammad, C.G. Chen, G. Balooch, E. Stebbins, C.R. McKenna, H. Davis, M. Niewolna, X.H. Peng, D.H. Nguyen, S.S. Ionova-Martin, J.W. Bracey, W.R. Hogue, D.H. Wong, R.O. Ritchie, L.J. Suva, R. Derynck, T.A. Guise, T. Alliston, Pharmacologic inhibition of the TGF-beta type I receptor kinase has anabolic and anti-catabolic effects on bone, PLoS ONE 4 (4) (2009) e5275.
[48] S.Y. Tang, T. Alliston, Regulation of postnatal bone homeostasis by TGFbeta, Bonekey Rep. 2 (2013) 255.
[49] M.A. Karsdal, M.S. Fjording, N.T. Foged, J.M. Delaisse, A. Lochter, Transforming growth factor-beta-induced osteoblast elongation regulates osteoclastic bone resorption through a p38 mitogen-activated protein kinase- and matrix metalloproteinase-dependent pathway, J. Biol. Chem. 276 (42) (2001) 39350–39358.
[50] J.P. Rys, D.A. Monteiro, T. Alliston, Mechanobiology of TGFbeta signaling in the skeleton, Matrix Biol. 52-54 (2016) 413–425.
[51] S. Hughes, J. Magnay, M. Foreman, S.J. Publicover, J.P. Dobson, A.J. El Haj, Expression of the mechanosensitive 2PK+ channel TREK-1 in human osteoblasts, J. Cell. Physiol. 206 (3) (2006) 738–748.
[52] X. Chen, C.M. Macica, K.W. Ng, A.E. Broadus, Stretch-induced PTH-related protein gene expression in osteoblasts, J. Bone Miner. Res. 20 (8) (2005) 1454–1461.
[53] Y. Liu, Y. Yang, L. Ding, Y. Jia, Y. Ji, LncRNA MIR4435-2HG inhibits the progression of osteoarthritis through miR-510-3p sponging, Exp. Ther. Med. 20 (2) (2020) 1693–1701.
[54] M.G. Johnson, K. Konicke, J. Kristianto, A. Gustavson, R. Garbo, X. Wang, B. Yuan, R.D. Blank, Endothelin signaling regulates mineralization and posttranscriptionally regulates SOST in TMOb cells via miR 126-3p, Physiol. Rep. 5 (4) (2017).
[55] B. Nam, H. Park, Y.L. Lee, Y. Oh, J. Park, S.Y. Kim, S. Weon, S.H. Choi, J.H. Yang, S. Jo, T.H. Kim, TGFbeta1 suppressed matrix mineralization of osteoblasts differentiation by regulating SMURF1-C/EBPbeta-DKK1 Axis, Int. J. Mol. Sci. 21 (24) (2020).
[56] J. Li, L. Xiang, X. Jiang, B. Teng, Y. Sun, G. Chen, J. Chen, J.V. Zhang, P.G. Ren, Investigation of bioeffects of G protein-coupled receptor 1 on bone turnover in male mice, J. Orthop. Translat. 10 (2017) 42–51.
[57] Y. Xin, C. Li, Y. Guo, R. Xiao, H. Zhang, G. Zhou, RNA-Seq analysis reveals a negative role of MSMO1 with a synergized NSDHL expression during adipogenesis of 3T3-L1, Biosci. Biotechnol. Biochem. 83 (4) (2019) 641–652.
[58] N. Hoggard, S. Bashir, M. Cruickshank, J.D. Miller, J.R. Speakman, Expression of neuromedin B in adipose tissue and its regulation by changes in energy balance, J. Mol. Endocrinol. 39 (3) (2007) 199–210.
[59] N.A. Cross, S. Chandrasekharan, N. Jokonya, A. Fowles, F.C. Hamdy, D.J. Buttle, C.L. Eaton, The expression and regulation of ADAMTS-1, -4, -5, -9, and -15, and TIMP-3 by TGFbeta1 in prostate cells: relevance to the accumulation of versican, Prostate 63 (3) (2005) 269–275.
[60] G.F. Le Bras, C. Taylor, R.B. Koumangoye, F. Revetta, H.A. Loomans, C.D. Andl, TGFbeta loss activates ADAMTS-1-mediated EGF-dependent invasion in a model of esophageal cell invasion, Exp. Cell. Res. 330 (1) (2015) 29–42.
[61] T. Lind, N. McKie, M. Wendel, S.N. Racey, M.A. Birch, The hyalectan degrading ADAMTS-1 enzyme is expressed by osteoblasts and up-regulated at regions of new bone formation, Bone 36 (3) (2005) 408–417.
[62] X. Li, H. Liu, L. Qin, J. Tamasi, M. Bergenstock, S. Shapses, J.H. Feyen, D.A. Notterman, N.C. Partridge, Determination of dual effects of parathyroid hormone on skeletal gene expression in vivo by microarray and network analysis, J. Biol. Chem. 282 (45) (2007) 33086–33097.
[63] K.M. Cawley, N.C. Bustamante-Gomez, A.G. Guha, R.S. MacLeod, J. Xiong, I. Gubrij, Y. Liu, R. Mulkey, M. Palmieri, J.D. Thostenson, J.J. Goellner, C.A. O'Brien, Local production of osteoprotegerin by osteoblasts suppresses bone resorption, Cell Rep. 32 (10) (2020) 108052.
[64] M. Tsukasaki, T. Asano, R. Muro, N.C. Huynh, N. Komatsu, K. Okamoto, K. Nakano, T. Okamura, T. Nitta, H. Takayanagi, OPG Production matters where it happened, Cell Rep. 32 (10) (2020) 108124.
[65] K.B. Jonsson, A. Frost, O. Nilsson, S. Ljunghall, O. Ljunggren, Three isolation techniques for primary culture of human osteoblast-like cells: a comparison, Acta Orthop. Scand. 70 (4) (1999) 365–373.
[66] T. Lind, A. Sundqvist, L. Hu, G. Pejler, G. Andersson, A. Jacobson, H. Melhus, Vitamin a is a negative regulator of osteoblast mineralization, PLoS ONE 8 (12) (2013) e82388.
[67] E.F. Bernstein, L.W. Fisher, K. Li, R.G. LeBaron, E.M. Tan, J. Uitto, Differential expression of the versican and decorin genes in photoaged and sun-protected skin. Comparison by

immunohistochemical and northern analyses, Lab. Invest. 72 (6) (1995) 662–669.
[68] C. Li, W.H. Wong, Model-based analysis of oligonucleotide arrays: expression index computation and outlier detection, Proc. Natl. Acad. Sci. U. S. A. 98 (1) (2001) 31–36.
[69] R.A. Irizarry, B. Hobbs, F. Collin, Y.D. Beazer-Barclay, K.J. Antonellis, U. Scherf, T.P. Speed, Exploration, normalization, and summaries of high density oligonucleotide array probe level data, Biostatistics 4 (2) (2003) 249–264.
[70] G.K. Smyth, Linear models and empirical bayes methods for assessing differential expression in microarray experiments, Stat. Appl. Genet. Mol. Biol. 3 (2004) Article3.
[71] G.K. Smyth, limma: linear Models for Microarray Data, in: R. Gentleman, V.J. Carey, W. Huber, R.A. Irizarry, S. Dudoit (Eds.), Bioinformatics and Computational Biology Solutions Using R and Bioconductor, Springer New York, New York, NY, 2005, pp. 397–420.
[72] Y. Benjamini, Y. Hochberg, Controlling the False Discovery Rate - a Practical and Powerful Approach to Multiple Testing, J R Stat Soc B 57 (1) (1995) 289–300.
[73] D.W. Huang, B.T. Sherman, R.A. Lempicki, Systematic and integrative analysis of large gene lists using DAVID bioinformatics resources, Nat. Protoc. 4 (1) (2009) 44–57.
[74] D.W. Huang, B.T. Sherman, R.A. Lempicki, Bioinformatics enrichment tools: paths toward the comprehensive functional analysis of large gene lists, Nucleic. Acids. Res. 37 (1) (2009) 1–13.